The International Journal of Advanced Manufacturing Technology (2018) 96:2525–2537
https://doi.org/10.1007/s00170-018-1593-x

ORIGINAL ARTICLE

An accurate thermal performance modeling and simulation method for motorized spindle of machine tool based on thermal contact resistance analysis

Yi Cui [1,2] · Haolin Li [2] · Tianjian Li [2] · Long Chen [2]

Received: 26 April 2017 / Accepted: 9 January 2018 / Published online: 23 February 2018

Abstract
Motorized spindle is an inevitable choice of precision machine, but it has a prominent heat problem for its specific configuration of build-in motor. The paper proposed temperature distribution and thermal deformation modeling and a thermal-structural coupling simulation analysis method for a motorized spindle system from a vertical machining center. In order to establish an accurate finite element model, the boundary condition of joint thermal contact resistance (TCR) was taken into account. The paper detailed on how to obtain the TCR value which is related to the machine tool parameters by means of experimental and theoretical methods, and carried out a simulation experiment for the purpose of acquiring a quantitative analysis of the TCR influence on the temperature results. In order to verify the effectiveness of the TCR relevant methods, the experiment was carried out. The agreement between the experimental results and the simulation results showed that the proposed method can more accurately simulate the thermal characteristics of the motorized spindle.

Keywords Motorized spindle · Thermal-structural coupling analysis · Temperature distribution · Thermal deformation · Thermal contact resistance

1 Introduction

Ultra-precision machine tool is primarily used to generate high-quality and functional parts usually made from hard and difficult to machine materials. The products have high surface finish, high form accuracy, and surface integrity for the electronic and optical industries as well as for astronomical applications [1]. Today, the overwhelming majority of ultra-precision machine tools are equipped with motorized spindles. Unlike externally driven spindles, the motorized spindles do not require mechanical transmission elements like gears and couplings. Such configuration makes it possible to achieve the precise control of the rotational movement of spindle [2]. But, because of motorized spindle being equipped with a built-in motor, it can bring large amounts of heat. The very high heat dissipation pushes other spindle components to their limits. Not only are individual components subject to more severe mechanical and thermal conditions, but spindle design grows more and more complex with added auxiliary components such as cooling, lubrication, and balancing system. In terms of the motorized spindle, thermal error problems seem to be more prominent [3]. Eventually, their thermal and mechanical behavior has become very difficult to calculate efficiently [4].

So, nowadays, more frequently machine tool builders take responsibility for the control of thermally induced displacements. This change takes place because machine tool users realized that comparable machine tools can show significantly different thermal errors and, in some machine tools, most of the energy supplied to the machine tool is used to stabilize the temperatures. Therefore, how to improve machine tool thermal performance by reducing thermal deformation and increase its machining accuracy is one of the most important research topics in machine tool design and performance optimization analysis.

✉ Yi Cui
cuiyi@usst.edu.cn

[1] School of Optical-Electrical and Computer Engineering, University of Shanghai for Science and Technology, No 516, Jungong Road, Shanghai 200093, China

[2] College of Mechanical Engineering, University of Shanghai for Science and Technology, No 516, Jungong Road, Shanghai 200093, China

Many scientists dedicated themselves to researching on thermal error analysis of machine tools. The relevant research can be summarized into three main categories. The first category is the analytical model, which is often used to establish the relationship between heat generation and temperature field. The model is based on Jaeger's moving heat source analysis: it can calculate the interface temperature distribution due to frictional heat source at the tool–workpiece interface in the metal cutting, surface grinding, or polishing processes. The tool is regarded as a moving fraction heat source which has a uniform or nonuniform distribution of heat flux intensity. Kuo et al. [5] proposed an analytical model to calculate the temperature rise in surface grinding. They reported that the difference between the calculated and experimental value is always less than 4%. Chen et al. [6] investigated the interface temperature rise in polishing a polycrystalline diamond (PCD) surface. Jaeger's moving heat source analysis was applied to determine the fractions of heat flux flowing into the PCD asperities and their counterpart in contact sliding and to give rise to the average temperature rise. The disadvantage of this method is that it can only compute the problems which have very simple boundary conditions. For the thermal characteristic of the motorized spindle system, it cannot render to an analytical solution because the geometric structure and boundary condition of the motorized spindle system are complex.

The second category is the empirical-based model. The empirical-based model is based on the assumption that thermal errors can be considered as a function of some critical discrete temperature points on the machine. It believes that the thermal deformation is associated with the temperature field and a few critical temperature points on the machine can be employed to sufficiently predict the temperature field of the entire machine [7]. The test system of the machine tool should be established firstly, and the temperature and deformation information is collected by the test system. And based on these measured data, a relationship between the thermal errors and temperature changes can be established using a proper mathematical method.

Different mathematical methods based on linear expansion models, rigid body models, neural networks, or other models have been employed to analyze the data obtained [8–10]. Once the mathematical model is established, the thermal performance of the machine tool under various conditions can be estimated. Chen et al. [11] proposed an auto-regression dynamic thermal error model which considers the temperature history and spindle-speed information to build accurate and robust models. And a further study combines the temperature measurements, spindle speed, and displacement measurement as the variables of the model. The experimental results show that the proposed displacement-based model has much better accuracy and robustness than the temperature-based model. Abdulshahed et al. [12] employed an adaptive neuro-fuzzy inference system with fuzzy c-means (FCM) clustering (FCM-ANFIS) to design the thermal prediction model. The model can achieve the best performance in terms of the accuracy of its predictive ability. Liu et al. [13] used the ridge regression algorithm to establish a thermal error model to inhibit the bad influence of collinearity on the thermal error-predicted robustness. They used the correlation coefficient to measure the correlation between temperature-sensitive points and thermal error. The algorithm can enhance the long-term predicted accuracy and robustness of thermal error.

After establishing the exact mathematical model of thermal error, the error values as a compensation signal are sent to the CNC controller. And through the readjustment of the axis positioning, the thermal error compensation is realized [14–16]. Although the compensation is an important method to reduce the thermal error, the cost of the test system is high. And the selection of mathematical models for thermal error has great randomness. It is difficult to determine whether the mathematical model is applicable to the specific machine tool or not. Therefore, it is hard to guarantee the accuracy of the predicted value of the thermal error. Most importantly of all, it belongs to the afterwards remedy method; the precision of the machine tool is basically qualitative. The space by the compensation to improve the precision of the machine tool is very limited.

The third category is the simulation of thermal performance and the establishment of a finite element model, which is a virtual prototype for thermal error analysis of the machine tool. This method is mainly used to optimize the design of machine tools [17, 18]. The typical process of using the simulation method to develop the machine tool design is shown in Fig. 1.

Zhao et al. [19] dynamically simulated the temperature field and thermal errors of the spindle using the finite element method, and built a robust thermal error model by selecting thermal key points. Holkup et al. [20] and Zahedi et al. [21] proposed a thermo-mechanical model of spindles. The model allows the prediction of temperature distribution and thermal growth, together with transient changes in bearing stiffness and contact loads under specified operating conditions. Creighton et al. [22] finished an analysis of thermal errors in a high-speed micro-milling spindle. The FEA correlates the temperature rise to the resulting structural deformation. And the structural deformation along with temperature change was experimentally obtained. Uhlmann et al. [23] present a 3D FEM model to predict the thermal behavior of a high-speed motor spindle. This model allows a transient simulation. And the verification experiments were implemented on a test spindle. Liu et al. [24] firstly established thermal-mechanical models of rotating ring geometry and interference-assembled rotating ring geometries, for thermal variation modeling of relative ring displacements of short cylindrical roller bearing and angular contact ball bearing. Then they associated these thermal variation models with a heat-fluid-solid coupling finite element simulation technique, to model spindle linear thermal errors and angular thermal errors.

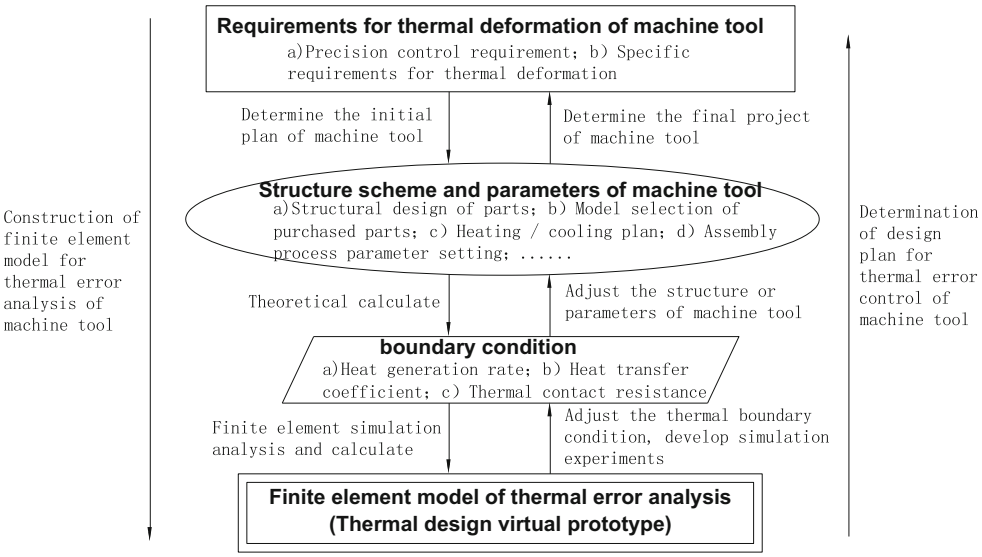

Fig. 1 The typical process for thermal error simulation analysis and control of the machine tool

The value of establishing a precise virtual prototype for enterprises is to predict whether the machine design meets the thermal design requirements in advance. According to the simulation results, the advantages and disadvantages of different design schemes can be compared, and the failure design because of poor thermal characteristics of the machine tool is avoided to the greatest extent. The second application value of the finite element method to the machine tool designer is that it can help the enterprise users to explore the optimal boundary conditions in light of thermal-error management. Based on the established finite element model, a large number of simulation experiments are carried out and the thermal sensitivity analysis of the boundary conditions can be used to realize the above functions. According to the simulation results, it provides reference for the enterprise users to adjust the design parameters of machine tools. Finally, this method can avoid costly design modifications in later stages of machine development based on experimental studies. Generally speaking, this method can improve the rationality of the design, and can greatly reduce the manufacturing cost of the enterprise.

The method of finite element analysis is highly demanding for the performance of the computer. And the processing power of state of the art personal computers is high enough to handle such computing requirements. Today, the ambition of every designer of highly efficient machine tools, particularly the ones to be used for precision machining, is to be able to accurately predict thermal errors through numerical simulations.

Although many scientists have made many researches on the analysis of machine tool spindle system thermal characteristics and have tried to establish better calculation models to obtain accurate simulation results, these papers rarely considered the influences from thermal contact resistance among the machine tool joints. A machine tool is such a case that the heat generated in the machine flows through mechanical joints and structural linkages which involve contacting surfaces. According to the contact pressure distribution of the joint which is dependent on the machine tool parameters such as material properties, surface finish of the joint interface, machining type of the joint interface, flatness deviations at the joint interface, initial loading type (tightness of fixing bolts, and force applied to the joint), and type of relative movement between the contacting components, the machine tools exhibited significantly different temperature gradients and thermal deflection. It is necessary to carry out experimental and theoretical research on obtaining thermal contact resistance values for the structural joints of the machine tool and then to study the quantitative influence degree of thermal contact resistance values on the temperature distribution and thermal deformation of the machine tool. These contents are the focus of this article.

This paper proposed and constructed an entire motorized spindle system's thermo-structural behavior simulation method. Specifically in the process, there are three steps. The first step is to build up the thermal performance simulation model, including structural model simplification, mesh generation, material properties applying, etc. The second step is to carry out the analysis of the heat transfer mechanism, including calculating the thermal sources, heat transfer coefficients, and thermal contact resistance values. And in the third step, applying the calculation values as boundary conditions to the model, thermal-structural coupling finite element simulation analysis of the spindle system was done. In the process, the temperature distribution analysis was calculated and then the nodes' temperature result from the previous step as body load was applied to the structural analysis. At last, the deformation distribution was obtained.

Especially, the article took into account the appropriate parameters of the machine tool joints and structural linkages, which detailed the experimental and theoretical methods to

calculate the TCR value. And a comparison between the simulation temperature result with and without the thermal contact resistance boundary conditions was done.

Lastly, in order to check the correctness of the proposed methods and the finite element simulation, in the paper the experimental research of the machine tool was carried out. And the thermal performance experimental platform was introduced. The temperature sensors were used to obtain the temperature field as well as capacitive displacement sensors for displacement of TCP.

2 Analysis of the motorized spindle thermal performance simulation method

2.1 Thermal performance simulation model

The paper focuses on a motorized spindle which is designed for a high-speed and precision vertical machine center. Figure 1 is the schematic of the motorized spindle system. An internal water-cooling spindle motor from SIEMENS is adapted. The rated power of the motor is 28 kW, the synchronous speed is 4200 rpm, the maximum speed is 20,000 r/min, and the torque is 63 Nm. The bearings adopted in the system are SKF ceramic ball bearings. Both the front bearings and the bear bearings use a coupled bearing pattern to support the system. Specifically, the front bearings are double row angular contact ceramic ball bearing, and the bear bearings are ceramic deep groove ball bearings. The specific structure of the motorized spindle is shown in Fig. 2.

The motorized spindle model is established by INVENTOR. Before mesh generation, a geometric model needs to be simplified. The general simplifying rules include changing chamfer into the right angle, and ignoring tiny structures such as the tool escape, thread holes, porosity, oil hole, etc. Then, the INVENTOR model is introduced into HYPERMESH. It is because compared with the tetrahedron element, the hexahedron element has the unparalleled advantages in many aspects, including the calculation precision, deformation characteristics, mesh quantity, anti-distortion level, number of mesh regeneration, etc. So, in the process of mesh generation all of the bodies are meshed into hexahedron elements by first drawing the surface mesh, and then using spin and drag function to generate volume mesh. After the mesh generation, the finite element model is produced, shown in Fig. 3. As far as the element type is concerned, 3D eight-node solid heat transfer elements that are compatible with stress analysis are used for the modeling of the spindle.

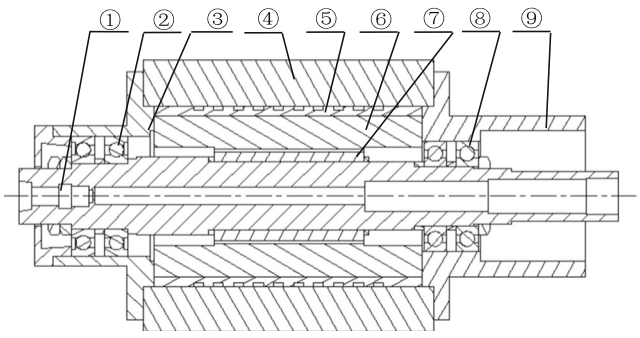

Fig. 2 The structure of the motorized spindle system. ① Rotating shaft. ② Double row angular contact ceramic ball bearing. ③ Front bearing cover. ④ Housing. ⑤ Cooling jacket. ⑥ Stator. ⑦ Rotator. ⑧ Ceramic ball bearing. ⑨ Rear bearing cover

2.2 The framework of thermal-structure coupling analysis of the motorized spindle system

After the finite element model is established, then it is imported into ANSYS to do the thermal-structure coupling analysis of the motorized spindle system. ANSYS provides two kinds of coupled thermal analysis methods: one is direct method and the other is indirect method. In the direct method, the coupling element which has both temperature and displacement degree of freedom is used. Both the thermal analysis result and the structural analysis result can be obtained simultaneously. This method has the characteristics of computing complexity and is time consuming. And it is suited for two-way coupling analysis. But for thermal deformation analysis of the spindle system, the effect of stress field to temperature field can be ignored, so the indirect method is adopted here. For the indirect method, the thermal analysis is calculated firstly, then the nodes' temperature result from the previous thermal analysis step as body load is applied for the structural analysis. For convenience, in the deformation field analysis process, the same geometric model and mesh model as the temperature field are used. And the temperature field analysis elements need to be changed into the corresponding structural analysis elements. Figure 4 is the framework of the thermal-structure coupling analysis of the spindle system.

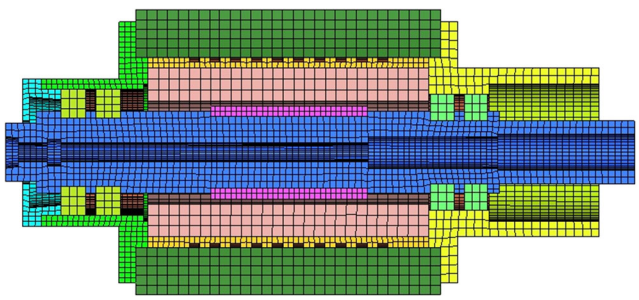

Fig. 3 The finite element model of the motorized spindle system

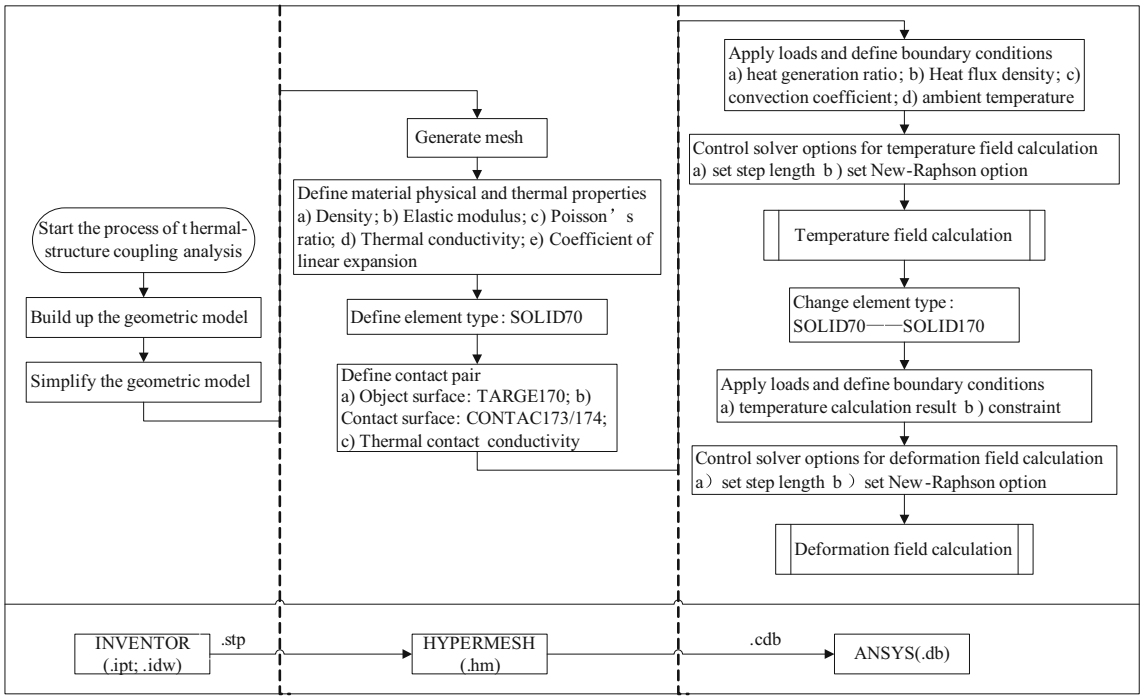

Fig. 4 The framework of thermal-structure coupling analysis of the motorized spindle system

3 Definition of the initial and boundary conditions

Heat transfer in the spindle system is a boundary value problem, so correct boundary conditions must be loaded to the spindle system in order to obtain a realistic solution. For the simulation of the thermal errors, it firstly needs to analyze the major thermal phenomena taking place in the spindle system as it operates. Figure 5 shows the heat sources and boundary conditions of the spindle system. The main heat sources are the motor and bearings. The boundary conditions include contact heat transfer within spindle parts and between spindle, spindle housing, and water cooling jacket for the motor stator as well as air convections at the gaps and convection to the ambient air.

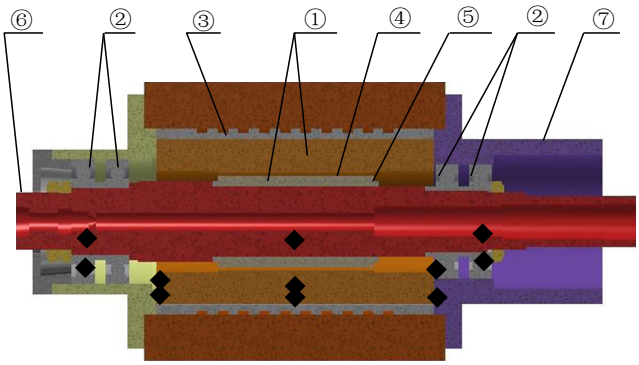

Fig. 5 Heat sources and boundary conditions of the motorized spindle system. ① Heat generation in the motor. ② Heat generation in the bearings. ③ Forced convection in the cooling jacket. ④ Surface heat exchange of air gap between stator and rotator. ⑤ The heat transfer coefficient of the rotator end. ⑥ Surface heat exchange of the rotating shaft. ⑦ Convection of ambient air. ♦ contact heat transfer

3.1 Heat resources

In the working process, the heat resources which affect the processing precision can be divided into two categories: one is internal heat resources and the other is outside heat resources. The practice shows that the internal heat resources are the main reasons which cause the thermal deformation. Internal heat resources include three parts, wastage heat of motor, frictional heat of bearings, and the operating heat. Because in the precision machining process, 95% of operating heat was carried away by scrap and cooling liquid, the thermal deformation influence from this part of heat source can be neglected.

Table 1 shows the type of the motor. And the heat generation rate of the motor stator and the rotor is the main thermal load of the motorized spindle thermal analysis. It can be calculated using Formula (1):

$$q = \frac{Q}{V} \tag{1}$$

where Q is the motor's heat power and V is the heat resource's volume. Motor wastage results in the heat generation of stator and rotator. The motor wastage (Q) is 3.6 kW. It is assumed that all motor wastage is converted to heat, and two thirds of the heat is produced by the

Table 1 The sizes of built-in motor

Motor type	L (mm)	D (mm)	D_A (mm)	d_i (mm)
1FE1083-4WN11BA	240	180	160	68

stator, one third by the rotator. And the volume of the rotator and stator V can be obtained directly from 3D models. The volumes of the rotator and the stator are 1207471 and 3,440,038 mm^3, respectively.

So according to Eq. (1), it can get the heat generation rate of the motor stator and the rotor; the results are shown in Table 2.

In the process of motorized spindle rotation, the intense friction between the ball and the inner and outer rings will inevitably generate a lot of heat. So, the frictional heat of high-speed bearings becomes another important heat source of the motorized spindle. The bearing friction heat power is calculated by Eq. (2) [25, 26]:

$$Q_f = 1.047 \times 10^{-4} Mn \tag{2}$$

where Q_f is the bearing friction heat power, M is the bearing friction torque, and n is the rotational speed, which is 2500 rpm.

For the high-speed bearing, the bearing friction torque can be calculated using Formula (3):

$$M = M_1 + M_2 \tag{3}$$

The friction torque M_1 relates to load, contact elastic deformation, and sliding friction. It can be calculated by Eq. (4):

$$M_1 = f_1 p_1 d_m \tag{4}$$

where f_1 is the load factor, the value of which is 1.95×10^{-4}, and p_1 is the load, in which for front and rear bearings, the p_1 values are 297.5 and 295.9 N, respectively. The bearing pitch diameter d_m is the average of the bearing inner and outer diameters; for front and rear bearings, they are 92.5 and 85 mm, respectively.

The friction torque M_2 depends on the rotational speed, the content of the lubricant, and the kinematic viscosity of the lubricant. It can be calculated by Eq. (5):

$$M_2 = 10^{-7} \times f_0 (\nu n)^{2/3} {d_m}^3 \tag{5}$$

where f_0 is the coefficient which accounts into the bearing structure and lubricant method used; here f_0 is 2 and ν is the kinematic viscosity of the lubricant under working temperature, the value of which is 2 mm^2/s at 40 °C.

The volume of bearing V can be obtained using Eq. (6):

$$V = \pi^2 d_m (D_b/2)^2 \tag{6}$$

where D_b is the diameter of the rolling element. For front and rear bearings, D_b values are 14.3 and 15 mm, respectively.

And the heat generation rate of frontal bearings and rear bearings is the other main thermal load of the motorized spindle thermal analysis. It can be calculated using Formula (7):

$$q = \frac{Q_f}{V} \tag{7}$$

According to the calculation method mentioned above and the relevant data, the heat generation rate of bearing can be obtained. They are shown in Table 3.

3.2 The heat transfer mechanisms

In the motorized spindle system, the major heat sinks include spindle housing, ambient air, motor cooling water, motor air, lubrication flow, etc. Through thermal conduction, convection, and radiation, heat transits from the heat source to the heat sinks happen.

Cooling water flows through a jacket in the shape of a helical duct. In order to facilitate mesh generation greatly, the geometry of the water duct is converted into one with a rectangular profile. The method of calculation of heat transfer coefficients for convection can refer to [27], and it is set to 290 W/(m^2·°C). From an applied view, the heat exchange coefficient on stator inner surface and rotor outer surface is equivalent. The heat transfer coefficient of the air gap between stator and rotator is 158 W/(m^2·°C). The heat transfer coefficient of the rotating shaft and the rotator end is 110 W/(m^2·°C) and 60 W/(m^2·°C), respectively. The value of $\alpha = 6$ W/(m^2·°C) is used for free convection around stationary surfaces. The same value is chosen for the heat transfer coefficient for the rear-end surface of shaft with surrounding air.

3.3 Machine thermal contact resistance analysis

Thermal contact resistance is the phenomenon of thermal behavior from one machine tool structural element to another which results in a temperature difference between the two

Table 2 The heat generation of built-in motor

Motor	Heat generation rate (W/m^3)
Stator	1,987,625
Rotator	348,833

Table 3 The heat generation of the bearing

Bearing	Heat generation rate (W/m^3)
Front	289,683
Rear	226,324

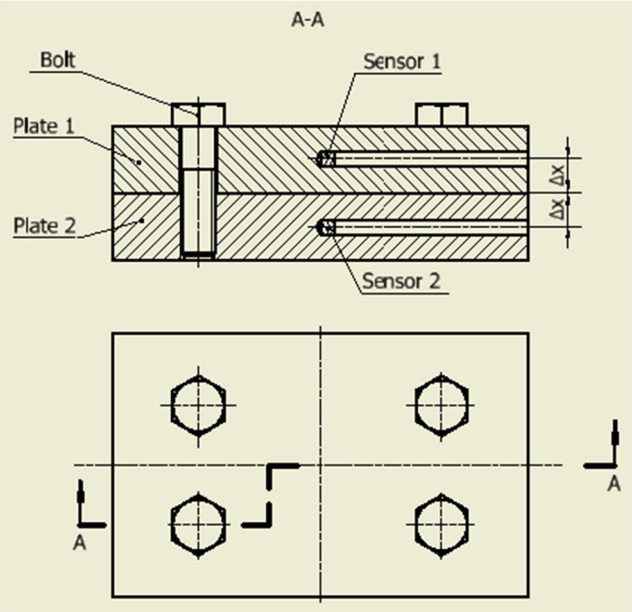

Fig. 6 The experiments to obtain the TCR value

contact surfaces. Contact heat transfer is a highly nonlinear behavior. To obtain reliable computational results from the simulation, the influences of the joint thermal contact resistance needed to be considered. The main parameters that influence thermal contact resistance include contact pressure, number of contact points, size and shape of contact points, size of voids, type of interfacial fluid in voids, pressure of interfacial fluids, hardness, flatness, modulus of elasticity, average surface finish, and surface cleanliness of contacting surfaces. So far, the TCR has been the most appropriate term to describe the phenomenon of how machine tool joints reduce heat flow.

Since the studies [28, 29] that were conducted to obtain thermal resistance values are limited to the selected material and the specific type of interface characteristics, the values are not readily transferable. Therefore, experiments were conducted to obtain the thermal resistance values for the structural joints of the machine.

The experiments to be established refer to the process described in literature [30]. In the experiment, the steel plates were used so that the values can be used for cast iron joints or steel-cast iron joints since the conductivity values for both steel and cast iron are very close. The interface of the steel plates has an average surface finish value Ra of 2 μm. The surface flatness was measured at 14 μm which is eliminated with a standard clamping force and therefore has negligible effect on the heat flow. Experiments were carried out using two rectangular steel plates. And both plates had the same dimensions of

$$\text{Length} = 0.145\ \text{m}, \text{Width} = 0.092\ \text{m}, \text{Height} = 0.0235.$$

In the testing procedure, plate-2 was heated and plate-1 clamped immediately onto the heated plate-2 using M14 bolts. The heater was turned off immediately after clamping plate-1. The torque value was 55 Nm, which was considered typical for machine tool joints. The aim is to measure temperature during the very initial phase when the heat energy from the bottom plate starts to propagate into the top plate through the interface to cause an increase in the temperature of the top plate. Figure 6 is the illustration of sensor positions within the plates.

The heat energy flowing from the lower plate to the top plate was calculated transiently using the heat transfer in Eq. (8):

$$Q' = mC_p(T_2 - T_1)/t + hA(T_{\text{surf}} - T_{\text{air}}) \tag{8}$$

where Q' is the energy transfer rate from the bottom plate to the top plate, m is the mass, and C_p is the specific heat capacity of the steel. T_2 is the inside temperature in the lower plate. T_1 is the inside temperature in the top plate. h is the convection coefficient, in a natural convection mode, and it was set to 6 W/(m^2·°C). A is the area of the plate. T_{surf} is the surface temperature of the top plate. T_{air} is the ambient temperature.

After determining the heat energy transfer through the plates, using the approach of one-dimensional steady

Table 4 Calculation of the thermal conductance

Notion	Symbol	Value
Mass of the plate (kg)	m	2.46
Specific heat capacity of the steel (J/(kg·°C))	C_p	460
Inside temperature in the top plate (°C)	T_1, T_{tp}	32.91
Inside temperature in the lower plate (°C)	T_2	34.22
Surface temperature of the top plate (°C)	T_{surf}	33.57
Ambient temperature (°C)	T_{air}	27.5
Energy transfer rate from the bottom plate to the top plate (W)	Q'	149
Conductivities of bottom and top plates (W/(m·°C))	k	52
Inside initial temperature in the lower plate (°C)	T_{bp}	44.92

Table 5 The material performance parameters of the spindle

Material	Density (g/cm^3)	Elastic modulus (GPa)	Poisson's ratio	Coefficient of thermal conductivity (W/(m·°C))	Coefficient of linear expansion (/°C)
Steel	7.85	210	0.3	52	1.2×10^{-5}
Cast iron	7.15	90	0.3	50	1.2×10^{-5}

conduction in a composite wall with contact resistance at the interface, the conductance h_c through the joint was calculated by Eq. (9) [30].

$$h_c = \frac{Q' k}{Ak\left(T_{bp} - T_{tp}\right) - 2Q'\Delta x} \tag{9}$$

where k is the conductivity of the bottom and top plates. Δx is the length of wall 1 and wall 2.

All calculations were performed transiently (10 s) for the time span to account for the nonlinear propagation of the energy from the bottom plate to the top plate. By combining the experimental data and formulas listed above, the thermal conductance value can be calculated as shown in Table 4.

The thermal conductance value (h_c) obtained was 1604 W/(m^2·°C). The result can be commonly used in joints of machine tools. This paper considered the thermal contact resistance for the main joints affecting machine transfer and deformation. As shown in Fig. 4, these thermal contact resistances were observed on the following joints: (1) rotating shaft and bearing, (2) bearing and bearing cover, (3) rotating shaft and rotator, (4) stator and cooling jacket, (5) cooling jacket and housing, (6) bearing cover and stator, and (7) bearing cover and cooling jacket.

The thermal contact conductance (TCC) value is the inverse of TCR [31]. By covering the contact element or target element in the contact interface and assigning the real constant thermal contact conductance value, HYPERMESH software can establish a contact model to simulate the thermal behavior across structural joints. The contact type developed in this paper belongs to the face to face contact. While ANSYS used the TARGE173 or TARGE174 element to simulate the contact surface, it used the TARGE170 element to simulate the target surface, which usually is the surface with high rigidity between the contact bodies. In the established model, the target element and contact element are face to face in normal direction.

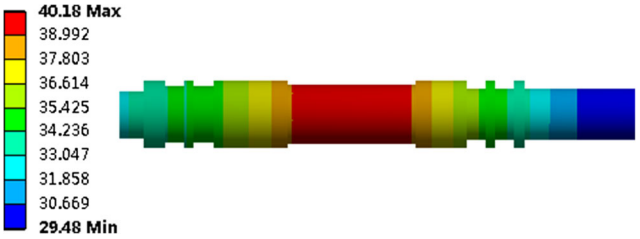

Fig. 8 Temperature distribution of the shaft with TCR

3.4 Definitions of the thermo-physical parameters for the machine tool materials

The material performance parameters of the spindle are shown in Table 5.

3.5 Discussion of thermal performance simulation results

To study the thermal performance of the spindle system, this paper performed temperature field and thermal deformation simulation analysis for a spindle system from the vertical machining center as an example. In the simulation examples, the environment temperature for the spindle system was set to 27.5 °C. And the rotational speed of the spindle was set to 2500 rpm. The boundary values obtained from Sects. 3.1 and 3.2 and the thermal contact resistance at the joints obtained from Sect. 3.3 are applied to the finite element model. The temperature field obtained from the thermal analysis and simulation is shown in Figs. 7 and 8.

From the temperature field plot in Figs. 7 and 8, it can be seen that when the spindle system reached the thermal equilibrium temperature field, and the maximum temperature value of the spindle system is 40.259 °C, the maximum temperature value of the shaft is 40.18 °C, which is almost the same as the temperature of the rotator. Although the motor wastage value of the rotator is only half of the

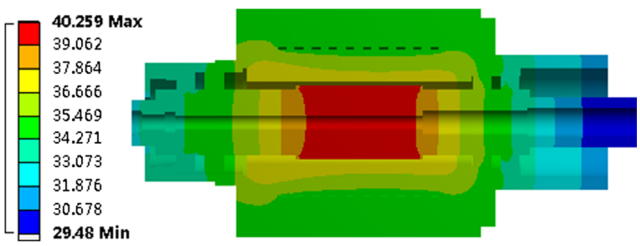

Fig. 7 Temperature distribution of the motorized spindle with TCR

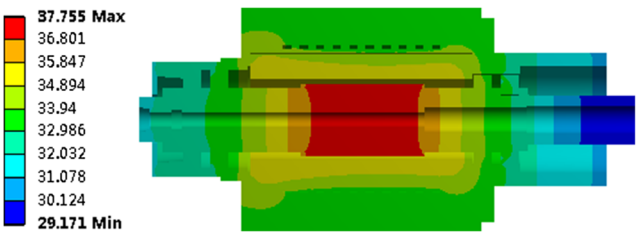

Fig. 9 Temperature distribution of the motorized spindle without TCR

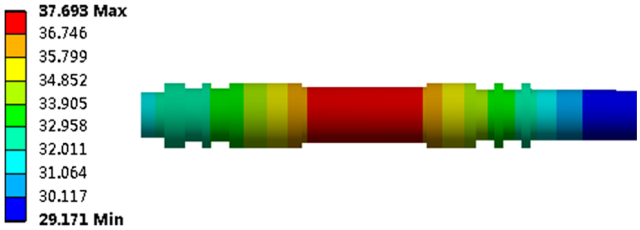

Fig. 10 Temperature distribution of the shaft without TCR

stator, the temperature of the rotator is higher than the temperature of the stator. It is the rotator's poor heat dissipation condition that leads to the result. At the same time, the phenomena illustrate the obvious effect of the forced cooling system in the motorized spindle.

In order to conduct a quantitative study of the effect from thermal contact resistance among the machine tool joints, a simulation experimentation was done. In the experimentation, the same boundary conditions and the heat load with the above simulation were applied to the finite element model of the machine tool spindle system, but the difference is that no thermal contact resistance boundary condition was applied. The simulation results without setting up the thermal contact resistance in the boundary conditions are shown in Figs. 9 and 10.

It can be seen that the maximum temperature value of the spindle system is 37.755 °C, and the maximum temperature value of the shaft is 37.693 °C. It can be summarized that whether the spindle system is loaded with thermal contact resistance or not has great influence on the thermal analysis results. Compared with the temperature result from without applying contact thermal resistance in the finite element model, the temperature value applying the contact thermal resistance is higher by 2–3 °C. Regardless of the TCR, it will result in the gap between the simulation result and the actual value. And this assumption is equivalent to defining the thermal conductivity of two contact surfaces is infinite. Such structure has the characteristics of fast heat dissipation velocity. The calculation of the temperature value is lower than that of the actual value.

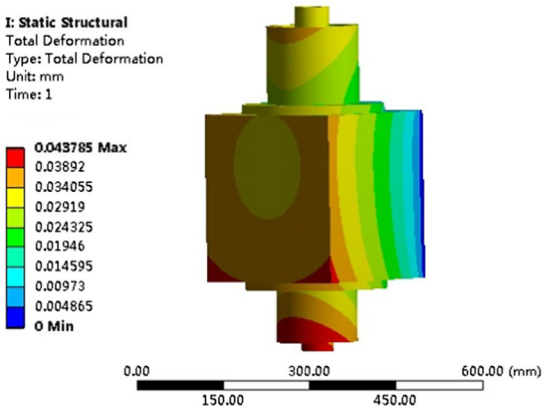

Total deformation

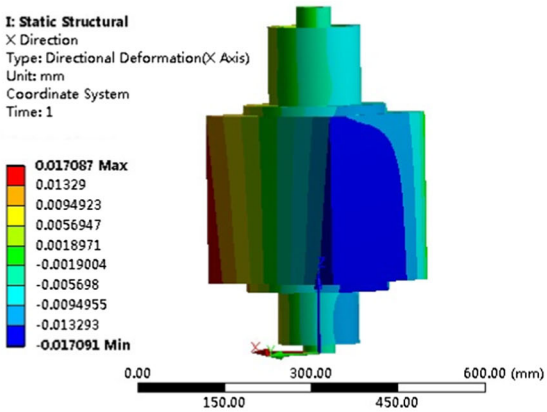

X directional deformation

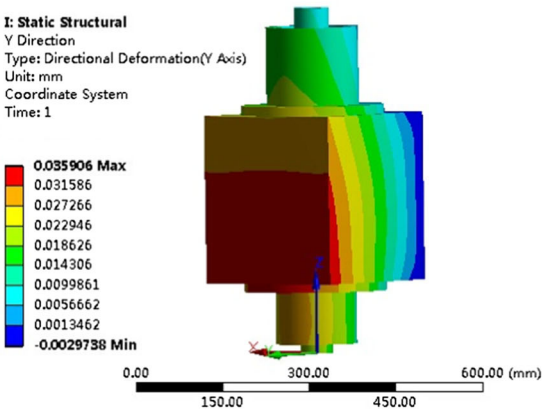

Y directional deformation

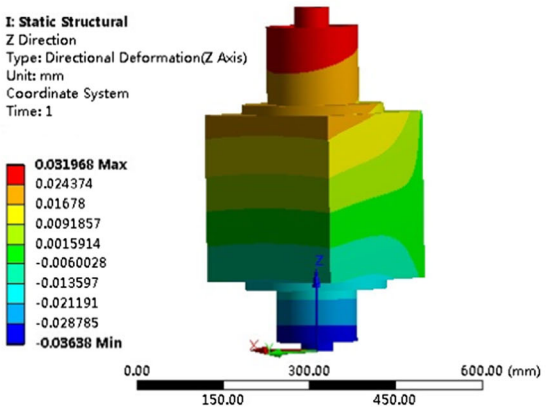

Z directional deformation

Fig. 11 Deformation distribution of the motorized spindle system

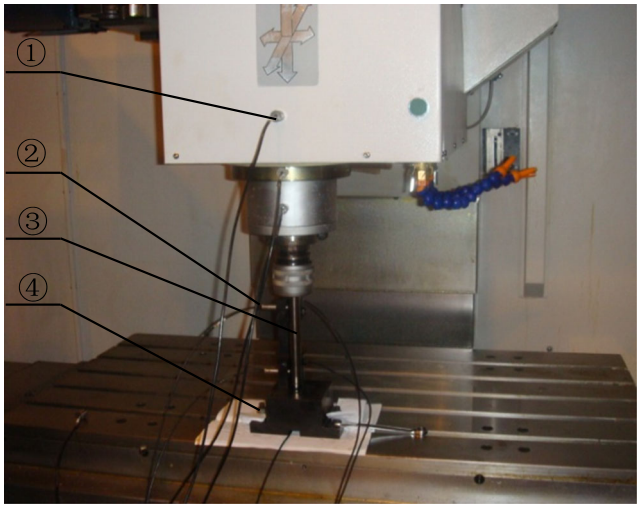

Fig. 12 The thermal performance experimental platform. ① Platinum resistance temperature sensor. ② Capacitive displacement sensor. ③ Test mandrel. ④ Fixture

From the simulation results, it can be seen that there exists a phenomenon of temperature jumping between the parts in the contact surfaces; it can be known that thermal contact resistance has a great effect on the machine internal heat conduction and the temperature distribution. In order to get more accurate machine tool thermal characteristics, it must be taken into consideration.

After the temperature field is calculated, the temperature field obtained through the simulation is used as the boundary condition, specifically the nodes' temperature result as the body load is applied to the structural analysis. The back of the spindle system being fixed, which is the constraint condition, the structural analysis of the spindle system was performed. The spindle system structural deformation obtained through the simulation under the influence of thermal loads is shown in Fig. 11.

From the deformation field plot in Fig. 8, it can be seen that the Y-directional deformation at the spindle nose reached 14 μm, and the Z-directional prolongation reached 36 μm. Because the spindle system is a symmetric structure in the X direction, the X-directional deformation at the spindle nose is zero.

4 Validation and discussion

4.1 Experiment setup

In order to verify the effectiveness of the proposed methods and the accuracy of finite element models, an experimental platform was set up based on a spindle system from a vertical machining center.

The experiment was established according to ISO 230-3 Test Code for Machine Tools—Part 3 [32]. The standardization provides the method for measuring thermal deformation caused by the rotation of the spindle of the machine tool. In the experiment, the measurement work of the temperature field and deformation field which is accrued by the heat generated from the rotating spindle of the machine tool were executed. The experimental platform is shown in Fig. 12.

In order to acquire the temperature field of the spindle system, nine PT100 platinum resistance temperature sensors were configured around the machine tool. Eight of them are used to measure motor, front bearing, rear bearing, and box temperature, and one for monitoring the environmental temperature. The displacement measuring system adopts CNDT6100 capacitive displacement sensors for thermal distortion caused by rotating spindles. There are five displacement sensors in the system; two of them are assigned to measure thermal deformation in the X direction, the other two of them are allocated to measure the Y direction, and the last one is used for the Z direction.

For the data acquisition equipment, a computer-based system is developed by LabVIEW. In it, all channels are sampled at once every 5 min, so continuously monitoring and recording all channels' information are achieved. The other auxiliary device includes a steel test mandrel and a fixture in which to mount the displacement sensors.

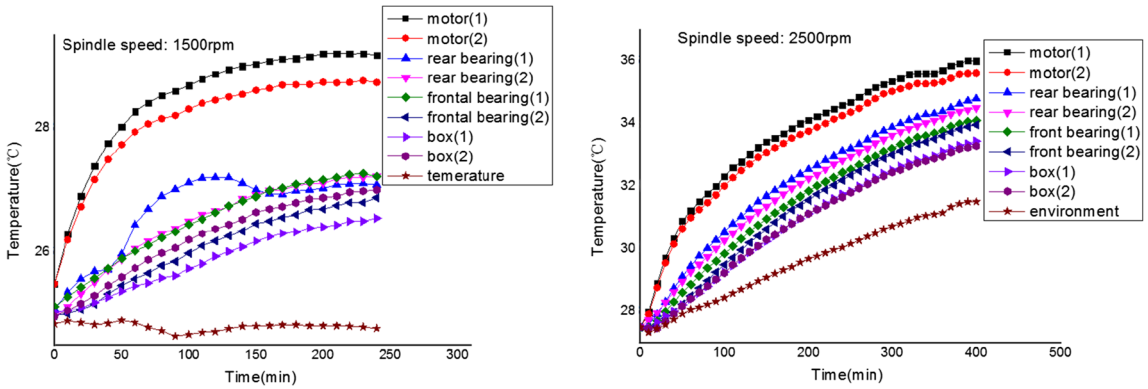

Fig. 13 The thermal temperature results in experiment

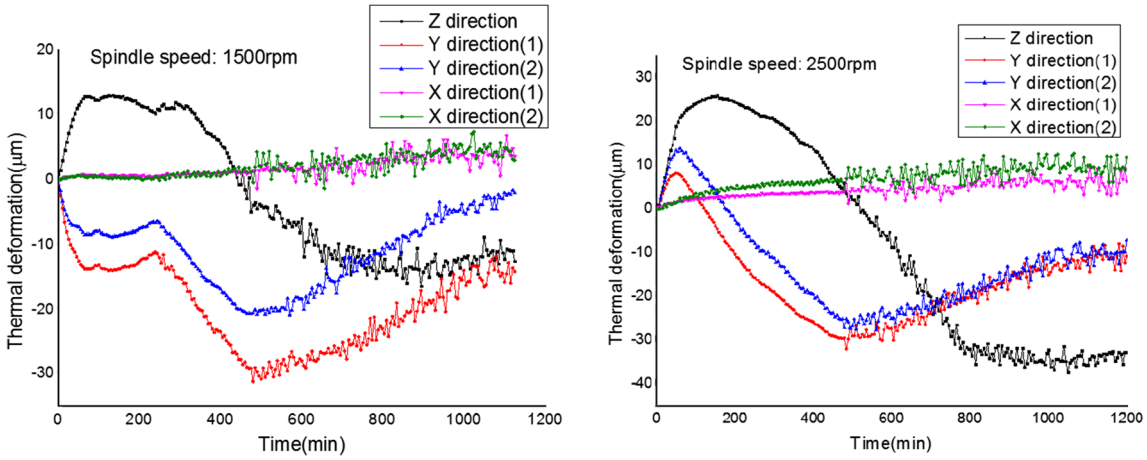

Fig. 14 The thermal deformation results in experiment

4.2 Experiment results

The experiment tests the thermal performance of the spindle in the temperature and deformation field with two aspects at the rotational speeds of 1500 and 2500 rpm, respectively. The experimental temperature results are shown in Fig. 13, and the deformation results are shown in Fig. 14.

The following can be seen from Fig. 13.

In the spindle system, the temperature at motor measuring points rises fastest, while the temperature rises are highest. The other measurement points displayed similar changes in temperature, the temperature rise is relatively slow.

As the speed increases, the corresponding measuring point temperature also increased. When the machine is in continuous operation and the speed is 1500 rpm, the machine has experienced 240 min to reach the thermal equilibrium state. When the speed is 2500 rpm, the equilibrium time is 400 min.

From the experiment, an interesting phenomenon was found. When the machine tool spindle operates at 2500 rpm, the ambient temperature with the machine temperature rise significantly increased. Before, environment temperature has been considered for machine tool temperature rise which is a major impact [33, 34]. Now it appears from the experimental results that the machine tool has a tremendous impact on the surrounding environment temperature. They both appear in an interactive influence. This may be because the environment temperature-measuring point location is arranged near the machine tool.

From Fig. 14, the following can be seen that.

The anisotropic thermal error of the machine tool increased significantly with the increase in rotational speed of the spindle. The changes in spindle speed have little effect on X-directional deformation. In different speeds, the changes in thermal error are basically the same in the Y direction. After a certain period of time of spindle rotation, there is an inflection point in the thermal deformation diagram. In the first stage, the spindle expands outward, and after being accumulated to a certain amount of deformation, the spindle starts to shrink to the opposite direction. As for the Z direction of the thermal deformation error, the displacement first linearly added up to a certain amount of deformation, and after a period of time, the spindle along the reverse direction continuously extent until it reached the equilibrium state.

4.3 Comparison of simulation and experimental results

In order to verify the accuracy of the simulation, the simulation results were compared with the results obtained from the experiments. First it selects temperature information coming from four representative measuring points to make a comparison with the value acquired from the experiment. They are

Table 6 Comparison of the simulation and experimental results of the temperature distribution

Spindle speed (rpm)	No. of the critical temperature measuring points	Experimental values (°C)	Simulation values (°C)	Simulation error (%)
2500	*T* (motor)	35.614	37.864	6.3%
	T (rear bearing)	34.5	36.666	6.3%
	T (frontal bearing)	33.962	35.469	4.6%
	T (box)	33.279	34.271	3.0%

Table 7 Comparison of the simulation and experimental results of the thermal deformations

Spindle speed (rpm)	Thermal deformation direction	Experimental values (μm)	Simulation values (μm)	Simulation error (%)
2500	X	6.3177	0	–
	Y	− 14.135	− 15.413	9.0%
	Z	− 32.8037	− 36.38	10.9%

motor, frontal bear, rear bear, and box-measuring points, respectively. And the results are shown in Table 6.

It can seen from Table 7 that the simulation and experimental values are in good agreement in temperature results, and the temperature error is limited in the range of 7%. The datum verified the correctness and effectiveness of the proposed thermal performance simulation model.

Then, a comparison was made between the simulated structural deformation data and the experimental data at the spindle nose measuring points from the X, Y, and Z directions; it is shown in Table 7.

From the table, one obvious problem is that an error in the X direction exists in the experiment column. And the higher the speed, the greater the error. But meanwhile the corresponding error in simulation column is zero. The cause of this phenomenon is that in the simulation, the research object is confined to the spindle system, and not to a whole machine. The spindle system in structure, source distribution, and boundary conditions exhibits symmetry properties in the X direction. But in the measuring process of the whole machine, the structure is not completely symmetrical. So in the test results, it appeared slightly offset, at approximately 6 μm.

For the Y direction and Z direction thermal deformations, the simulation results match the experiment datum very well. And the simulation error was less than 11%.

In a word, the consistence between the simulation and experiment datum illustrated the effectiveness of the proposed thermal performance simulation method. This method can accurately predict thermal errors of the machine tool through numerical simulations in later stages of machine development; it can help machine tool designers to compare different designs in early stages of development to achieve an optimization design.

5 Conclusions

This paper introduced how to obtain the thermal contact resistance by means of experimental and theoretical calculation methods; the thermal contact resistance value represents more appropriately for the joints of the machine tool under research.

Then the thermal contact resistance value was used as an important boundary condition to be loaded into the finite element simulation calculation of the thermal error of the motorized spindle system. And a quantitative comparison was obtained that the temperature of loading TCR is about 2–3 °C higher than the temperature that does not load TCR. Because of the TCR, the machine tool exhibited significantly different temperature gradients, and hence thermal deformation. It can be concluded that the influence of TCR can ot be ignored when doing thermal analysis of the spindle system.

In order to validate the correctness of the method to obtain the TCR value, the paper carried out an experimental study. The simulation error of the temperature fields was less than 7%, while the simulation error of the deformation in the Y and Z directions was less than 11%. The simulated spindle characteristics exhibited good agreement with the experimental results.

Considering the effect of TCR on the thermal error is of great significance for the designers of machine tools. This is because the TCR value depends on the machine tool parameters such as material properties, surface finish of the joint interface, machining type of the joint interface, flatness deviations at the joint interface, initial loading type (tightness of fixing bolts, and force applied to the joint), type of relative movement between the contacting components, etc. Based on the simulation model containing TCR boundary condition, the enterprise can carry out the thermal sensitivity calculation of the TCR relative to the thermal error of the machine tool, and explore the appropriate parameter (e.g., clamping force of fixing bolts) of the machine tool joints; these contents are also to be carried out in detail in a further study.

Acknowledgements The authors gratefully acknowledge the financial support provided by the Science and Technology Commission of Shanghai Municipality (Grant No. 15110502300).

References

1. Brinksmeier E, Mutlugünes Y, Klocke F, Aurich JC, Shore P, Ohmori H (2010) Ultra-precision grinding. CIRP Ann Manuf Technol 59(2):652–671. https://doi.org/10.1016/j.cirp.2010.05.001
2. Abele E, Altintas Y, Brecher C (2010) Machine tool spindle units. CIRP Ann Manuf Technol 59(2):781–802. https://doi.org/10.1016/j.cirp.2010.05.002
3. Mayr J, Jedrzejewski J, Uhlmann E, Donmez MA, Knapp W, Härtig F, Wendt K, Moriwaki T, Shore P, Schmitt R, Brecher C, Würz T, Wegener K (2012) Thermal issues in machine tools. CIRP Ann Manuf Technol 61(2):771–791. https://doi.org/10.1016/j.cirp.2012.05.008

4. Bossmanns B, Tu JF (1999) A thermal model for high speed motorized spindles. Int J Mach Tools Manuf 39(9):1345–1366. https://doi.org/10.1016/S0890-6955(99)00005-X
5. Kuo WL, Lin JF (2006) General temperature rise solution for a moving plane heat source problem in surface grinding. Int J Adv Manuf Technol 31(3-4):268–277. https://doi.org/10.1007/s00170-005-0200-0
6. Chen Y, Zhang LC, Arsecularatne JA, Montross C (2006) Polishing of polycrystalline diamond by the technique of dynamic friction, part 1: prediction of the interface temperature rise. Int J Mach Tool Manu 46(6):580–587. https://doi.org/10.1016/j.ijmachtools.2005.07.018
7. Yan JY, Yang JG (2009) Application of synthetic grey correlation theory on thermal point optimization for machine tool thermal error compensation. Int J Adv Manuf Technol 43(11–12):1124–1132. https://doi.org/10.1007/s00170-008-1791-z
8. Li JW, Zhang WJ, Yang GS (2009) Thermal-error modeling for complex physical systems: the-state-of-arts review. Int J Adv Manuf Technol 42(1-2):168–179. https://doi.org/10.1007/s00170-008-1570-x
9. Ramesh R, Mannan MA, Poo AN (2000) Error compensation in machine tools—a review part II: thermal errors. Int J Mach Tool Manu 40(9):1257–1284. https://doi.org/10.1016/S0890-6955(00)00010-9
10. Wang LP, Wang HT, Li TM, Li FC (2015) A hybrid thermal error modeling method of heavy machine tools in z-axis. Int J Adv Manuf Technol 80(1–4):389–400. https://doi.org/10.1007/s00170-015-6988-3
11. Chen JS, Hsu WY (2003) Characterizations and models for the thermal growth of a motorized high speed spindle. Int J Mach Tool Manu 43(11):1163–1170. https://doi.org/10.1016/S0890-6955(03)00103-2
12. Adbulshahed AM, Longstaff AP, Fletcher S (2015) Thermal error modelling of machine tools bases on ANFIS with fuzzy c-means clustering using a thermal imaging camera. Appl Math Model 39(7):1837–1852. https://doi.org/10.1016/j.apm.2014.10.016
13. Liu H, En MM, Wei XY, Zhuang XD (2017) Robust modeling method for thermal error of CNC machine tools based on ridge regression algorithm. Int J Mach Tool Manu 113:35–48. https://doi.org/10.1016/j.ijmachtools.2016.11.001
14. Gomez-Acedo E, Olarra A, Orive J (2013) Methodology for the design of a thermal distortion compensation for large machine tools based in state-space representation with Kalman filter. Int J Mach Tool Manu 75:100–108. https://doi.org/10.1016/j.ijmachtools.2013.09.005
15. Feng WL, Li ZH, Gu QY, Yang JG (2015) Thermally induced positioning error modelling and compensation based on thermal characteristic analysis. Int J Mach Tool Manu 93:26–36. https://doi.org/10.1016/j.ijmachtools.2015.03.006
16. Liu K, Sun MJ, Zhu TJ, Wu YL, Liu Y (2016) Modeling and compensation for spindle's radial thermal drift error on a vertical machining center. Int J Mach Tool Manu 105:58–67. https://doi.org/10.1016/j.ijmachtools.2016.03.006
17. Jiang S, Min X (2012) Thermal design of the vertical machining centre headstock by the forced cooling method. Proc Inst Mech Eng C J Mech Eng Sci 226(3):738–751
18. Sun LJ, Ren MJ, Hong HB, Yin YH (2017) Thermal error reduction based on thermodynamics structure optimization method for an ultra-precision machine tool. Int J Adv Manuf Technol 88(5–8):1267–1277. https://doi.org/10.1007/s00170-016-8868-x
19. Zhao HT, Yang JG, Shen JH (2007) Simulation of thermal behavior of a CNC machine tool spindle. Int J Mach Tool Manu 47(6):1003–1010
20. Holkup T, Cao H, Kolár (2010) Thermo-mechanical model of spindles. CIRP Ann Manuf Technol 59(1):365–368. https://doi.org/10.1016/j.cirp.2010.03.021
21. Zahedi A, Movahhedy MR (2012) Thermo-mechanical modeling of high speed spindles. Scientia Iranica B 19(2):282–293. https://doi.org/10.1016/j.scient.2012.01.004
22. Creighton E, Honegger A, Tulsian A (2010) Analysis of thermal errors in a high-speed micro-milling spindle. Int J Mach Tool Manu 50(4):386–393. https://doi.org/10.1016/j.ijmachtools.2009.11.002
23. Uhlmanna E, Hu J (2012) Thermal modelling of a high speed motor spindle. Procedia CIRP 1:313–318. https://doi.org/10.1016/j.procir.2012.04.056
24. Liu T, Gao WG, Zhang DW, Zhang YF, Chang WF, Liang CM, Tian YL (2017) Analytical modeling for thermal errors of motorized spindle unit. Int J Mach Tool Manu 112:53–70. https://doi.org/10.1016/j.ijmachtools.2016.09.008
25. Zhang JF, Feng PF, Chen C (2013) A method for thermal performance modeling and simulation of machine tools. Int J Adv Manuf Technol 68(5–8):1517–1527. https://doi.org/10.1007/s00170-013-4939-4
26. Zhao CL, Guan XS (2012) Thermal analysis and experimental study on the spindle of the high-speed machining center. AASRI Procedia 1:207–212. https://doi.org/10.1016/j.aasri.2012.06.032
27. Lu ZS, Ma BH (2009) Thermal model of hydrostatic motorized spindle. J Syst Simul 21(2):352–356
28. Jiang S, Zheng Y (2009) An analytical model of thermal contact resistance based on the Weierstrass–Mandelbrot fractal function. Proc Inst Mech Eng C J Mech Eng Sci 224:959–967
29. Jeng YR, Chen JT, Cheng CY (2003) Theoretical and experimental study of a thermal contact conductance model for elastic, elastoplastic and plastic deformation of rough surfaces. Tribol Lett 14(4):251–259. https://doi.org/10.1023/A:1022632801251
30. Mian NS (2010) Efficient machine tool thermal error modelling strategy for accurate offline assessment. Doctoral thesis, University of Huddersfield
31. Fang B, Gu TQ, Ye DP, Luo TZ (2016) An improved thermo-mechanical model for vertical machining center. Int J Adv Manuf Technol 87(9–12):2581–2592. https://doi.org/10.1007/s00170-016-8651-z
32. ISO 230-3 (2007) Test code for machine tools—part 3: determination of thermal effects. Genf, Schwitzerland
33. Tan B, Mao XY, Liu HQ, Li B, He SP, Peng FY, Yin L (2014) A thermal error model for large machine tools that considers environmental thermal hysteresis effects. Int J Mach Tools Manuf 82-83:11–20. https://doi.org/10.1016/j.ijmachtools.2014.03.002
34. Mian NS, Fletcher S, Longstaff AP (2013) Efficient estimation by FEA of machine tool distortion due to environmental temperature perturbations. Precis Eng 37(2):372–379